

Velocity Map Imaging of Dissociative Ionization and Coulomb Explosion of CH₃I Induced by a Femtosecond Laser

Yanmei Wang, Song Zhang, Zhengrong Wei, and Bing Zhang*

State Key Laboratory of Magnetic Resonance and Atomic and Molecular Physics, Wuhan Institute of Physics and Mathematics, Chinese Academy of Sciences, Wuhan 430071, People's Republic of China, and Graduate School of the Chinese Academy of Sciences, Beijing 100039, People's Republic of China

Received: November 20, 2007; In Final Form: January 21, 2008

The dissociative ionization and the Coulomb explosion of CH₃I irradiated by a 35 fs 800 nm laser with a laser intensity of 4×10^{13} to 6×10^{14} W/cm² was studied. In a relatively weak laser field (about 10^{13} W/cm²), the dissociative ionization of CH₃I took place. The speed distributions of the CH₃⁺ and I⁺ fragments were measured and fitted using multiple Gaussian functions. Different product channels were found for CH₃⁺ and I⁺, respectively. In a strong laser field (about 10^{14} W/cm²), the multiply ionized fragment ions of I^{q+} ($q \leq 3$), which experienced a Coulomb explosion, were observed. The angular and speed distributions of the I⁺, I²⁺, and I³⁺ fragments were obtained. All of these fragment angular distributions are anisotropic and peaked along the laser polarization direction. The I^{q+} ion angular distributions all were of similar widths, which would imply that the geometric alignment dominated the process, as opposed to a dynamic alignment mechanism.

1. Introduction

The interaction of intense laser radiation with molecules has attracted the interest of researchers because of the appearance of some new phenomena, such as multiphoton ionization (MPI),^{1,2} field ionization (FI),³ dissociation ionization (DI),⁴ and Coulomb explosion.^{5,6} In weak fields, the super-excited molecule may decay by direct ionization, dissociation to two neutral fragments, or DI to a neutral fragment, an ion, and an electron. The anisotropy of the fragment momentum depends in this limit on the direction of the transition dipole moment of the molecule. DI is inherently interesting because it is a multibody, two-continuum process that involves both electronic and nuclear motion.⁷ DI can result from collisions of molecules with either particles or photons. In the latter case, the detailed mechanism is very sensitive to the intensity and frequency of the electromagnetic field. In strong fields ($\geq 10^{14}$ W cm⁻²), electrons are successively removed by multiphoton excitation until the internuclear potential becomes essentially Coulombic, at which point a Coulomb explosion is ignited. The behavior of the molecule in this limit is dominated by the properties of the field. Anisotropy of the angular distribution of the recoiling fragments results from the fact that the mechanism of enhanced ionization⁸ depends on the angle between the symmetry axis of the neutral molecule and the polarization vector of the field. For different laser intensities, the physical mechanisms can be estimated according to the adiabatic parameter (AP)⁹

$$AP = \sqrt{IP / (1.87 \times 10^{-13} I_0 \lambda^2)} \quad (1)$$

where IP is the molecular ionization potential (electronvolts) in the absence of the laser field, I is the laser intensity (W/cm²), and λ is the laser wavelength (micrometers). AP values of > 1 imply the participation of a MPI mechanism. AP values

of < 1 imply the participation of a FI mechanism. In the case of 800 nm irradiation, the MPI process dominates the photochemistry of CH₃I molecules when the laser intensity is lower than 8×10^{13} W/cm².

Methyl iodide, as a typical molecule with C_{3v} symmetry, was investigated by a velocity map imaging method using a nanosecond laser at different wavelengths.^{10–13} The alignment of this molecule in intense laser fields has been investigated widely using time-of-flight mass spectroscopy (TOFMS).^{14,15} Graham et al.¹⁴ studied the angular distributions of fragment ions generated from the Coulomb explosion of methyl iodide with a 50 fs intense laser pulse (10^{16} W/cm²). Multiply charged iodine fragment ions up to I⁷⁺ were detected, and the kinetic energy releases (KERs) of the iodine ions were measured. Kaziannis et al.¹⁶ studied the dynamic alignment of CH₃I by a strong picosecond laser field with high-resolution TOFMS. Some Coulomb explosion channels were assigned, and the KERs of CH₃⁺ ions from different channels were measured. Liu et al.¹⁷ investigated the ionization and dissociation of CH₃I using a reflection TOF mass spectrometer in an intense laser field ($\leq 6.6 \times 10^{14}$ W/cm²). They found that the KERs of the fragment ions were independent of the laser intensity, and the possible Coulomb explosion channels were identified.

TOFMS has been used as a detection method in all the previously mentioned work. In this paper, we report our study on the DI and Coulomb explosion of CH₃I at different laser intensities using a velocity map imaging method. The velocity map imaging method,^{18,19} which can provide information on the speed and angular distributions of the target particles at the same time, have enabled new and detailed high-resolution investigations of the photodissociation and photoionization of a wide range of gas-phase molecules. On the basis of the high resolution of the velocity map imaging, the KERs of the fragment ions were determined with high precision. The DI was induced by a 1 kHz femtosecond laser pulse centered at 800 nm with a 43 nm bandwidth, and the laser intensity was $\sim 5 \times$

* To whom correspondence should be addressed. E-mail: bzhang@wipm.ac.cn; fax: +86-27-87198576.

10^{13} W/cm². The Coulomb explosion of CH₃I was produced by a 10 Hz femtosecond laser pulse centered at 800 nm with a 40 nm bandwidth at a laser intensity of $\sim 6 \times 10^{14}$ W/cm². The possible multiphoton DI channels and the alignment mechanism in the Coulomb explosion were discussed.

2. Experimental Procedures

The imaging experimental setup has been described in detail elsewhere.²⁰ Briefly, it consists of a home-built TOF mass spectrometer and a two-dimensional (2D) position sensitive detector. The TOF mass spectrometer is a differentially pumped vacuum chamber coupled with an electrostatic immersion lens. The chamber is divided into two stages by a 1 mm skimmer and maintained to a background pressure of 4×10^{-6} Pa.

A molecular beam was produced by seeding methyl iodide (99.5% purity) in helium gas at a backing pressure of 1 atm through a pulsed valve and intersected with a linearly polarized femtosecond laser in the reaction region located in the second stage of the vacuum chamber. The commercial femtosecond laser system consists of a Ti:sapphire oscillator (Coherent Int., Mira-seed) pumped by a CW second harmonic of an Nd:YVO₄ laser (Coherent Int., Verdi-5), which produced seed pulses of about 20 fs duration. The seed pulses temporally were stretched before being admitted into a chirped regenerative amplifier pumped by a Q-switched Nd:YLF laser with an average power of 8 W at a working frequency of 1 kHz. The chirped regenerative amplifier outputs long pulses (~ 150 ps) with 1.4 mJ per pulse at a working frequency of 1 kHz. The amplified long pulses subsequently were compressed to obtain short femtosecond pulses with a maximum energy of 1 mJ per pulse. The full wave at half-maximum (FWHM) of the output pulse was 35 fs. The 5×10^{13} W/cm² experiment was carried out from this output. Instead of seeding the picosecond pulses into the compressor, the stronger laser of 6×10^{14} W/cm² was produced by inducing the amplified long pulses (~ 150 ps) into a multipass amplifier (MPA, Coherent Int.) system, which was pumped by a flash-pumped Q-switched Nd:YAG laser (Powerlite 8000, Continuum) at a working frequency of 10 Hz. The output of MPA then was compressed by an outside two-grating system to be 35 fs pulses, centered at 800 nm with a 40 nm bandwidth. The horizontal laser output was set to be vertical by a half-wave plate and focused perpendicularly onto the ionization zone using a 250 mm focal length lens. The generated ions were extracted and accelerated by the electrostatic immersion lens and projected onto a 2D detector composed of a micro-channel plate (MCP)/phosphor screen and a charge-coupled device (CCD) camera. The TOF mass spectra were acquired using a photomultiplier tube (PMT). The occurrence of clusters was controlled by adjusting the sample expansion conditions.

The velocity map imaging was provided by a specially designed electrostatic immersion lens. A high-voltage pulse with a 1 μ s duration was applied to MCP to separate the needed ion signal from that of scattered laser light and background ions with different masses. The images were accumulated by 30 000 laser shots. A synchronous 1 kHz signal from the Synchronization and Delay Generator of the laser system was converted to a 10 Hz signal by an outer trigger box. This 10 Hz signal was divided into two. One was used to trigger the pump laser of MPA. The other was used to externally trigger our pulse generator (DG535, Stanford Research System), which was used to control the operation of the pulse valve and the application of the high-voltage pulse, to achieve synchronization.

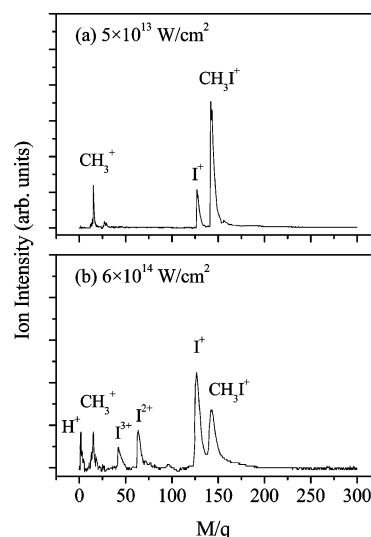


Figure 1. TOF mass spectra of CH₃I irradiated by 800 nm, 35 fs laser pulses at intensities of (a) 5×10^{13} W/cm² and (b) 6×10^{14} W/cm².

3. Results

3.1. TOF Mass Spectra. Two typical TOF mass spectra of the ions at different laser intensities are pictured in Figure 1 in the range of $M/q = 0-300$ au. The laser polarization was perpendicular to the TOF axis for both panels of Figure 1.

In Figure 1a, the mass spectrum at an intensity of 5×10^{13} W/cm², three strong peaks were found to be CH₃⁺, I⁺, and CH₃I⁺. The CH₃I⁺ peak was much stronger than the other two. More peaks were observed in the mass spectrum at an intensity of 6×10^{14} W/cm². Not only some singly charged ions including H⁺, CH₃⁺, I⁺, and CH₃I⁺ but multiply charged peaks corresponding to I²⁺ and I³⁺ occurred. This is the typical character of a Coulomb explosion in a strong laser field. In this condition, the parent ion CH₃I⁺ is weakened, and I⁺ becomes stronger. The area ratio of CH₃I⁺/I⁺ is 4:1 at 5×10^{13} W/cm² and 1:1 at 6×10^{14} W/cm², respectively. The I^{q+} ($q = 1, 2,$ and 3) ion intensity decreases with the increase of the charges. The area ratio of three I^{q+} ions is 8:2:1 for $q = 1, 2,$ and 3 . H⁺, which is not shown in Figure 1a, appears in Figure 1b in a stronger laser field.

3.2. Speed and Angular Distributions. The raw images, representing two-dimensional projections of the original three-dimensional speed/angular distributions, obtained following the interaction of a femtosecond laser pulse with sample molecules, are displayed in Figures 2 and 3. The polarization vector of the laser is parallel to the vertical direction of the image plane.

It is obvious that not only the images of CH₃⁺ and I⁺ products in a relatively weaker laser field of 5×10^{13} W/cm² but also the images of I⁺, I²⁺, and I³⁺ products in a laser field of 6×10^{14} W/cm² show a strong anisotropy along the polarization vector of the excitation laser. The images of the parent ion are small spots at the center of the phosphor screen in two cases. They are characteristically isotropic and are not shown here.

Using the inverse Abel transform method, a full three-dimensional fragmentation image could be reconstructed. From the inversed images, $P(v)$, the speed distributions of the detected ions, which were derived by integrating over all angles for each speed, are shown in Figures 2 and 3. The center-of-mass translational energies were calculated from the energy and momentum conservation relations using the velocities obtained from the I^{q+} and CH₃⁺ images.

The speed distributions of CH₃⁺ and I⁺ ions, which were produced in a relatively weaker laser field, both can be fitted

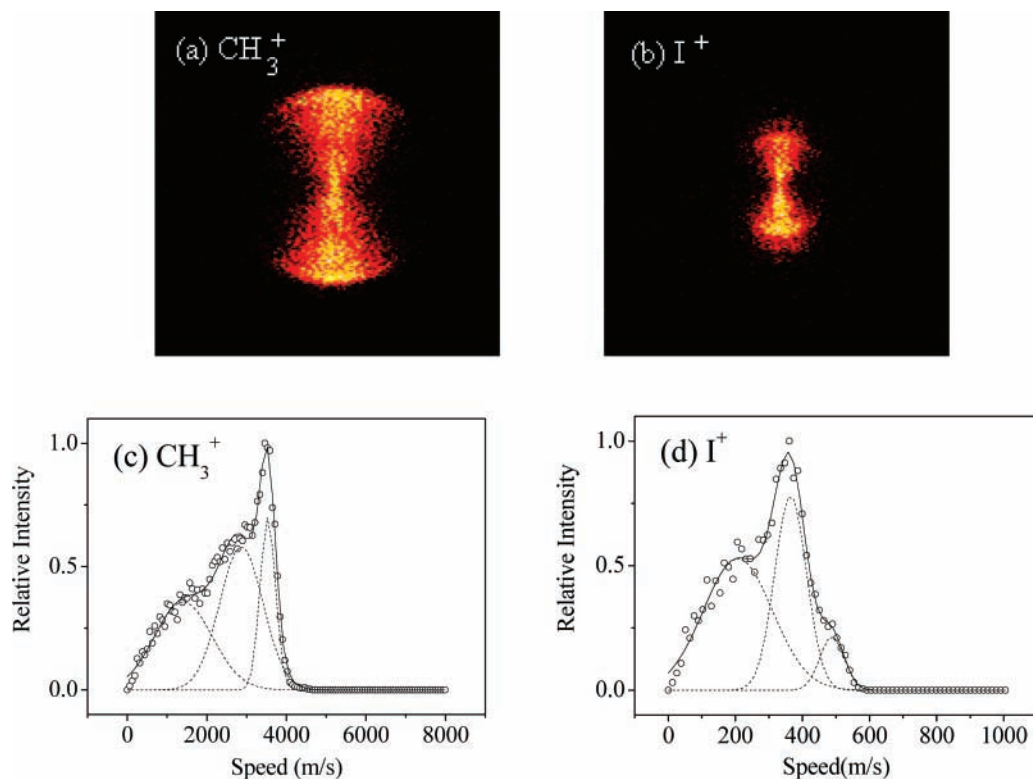


Figure 2. Images and speed distributions of CH_3^+ and I^+ at a laser intensity of $5 \times 10^{13} \text{ W/cm}^2$. Dashed lines (----) show the fitting lines. The solid line (—) is a sum of the simulated distributions, and the circles represent the experimental results.

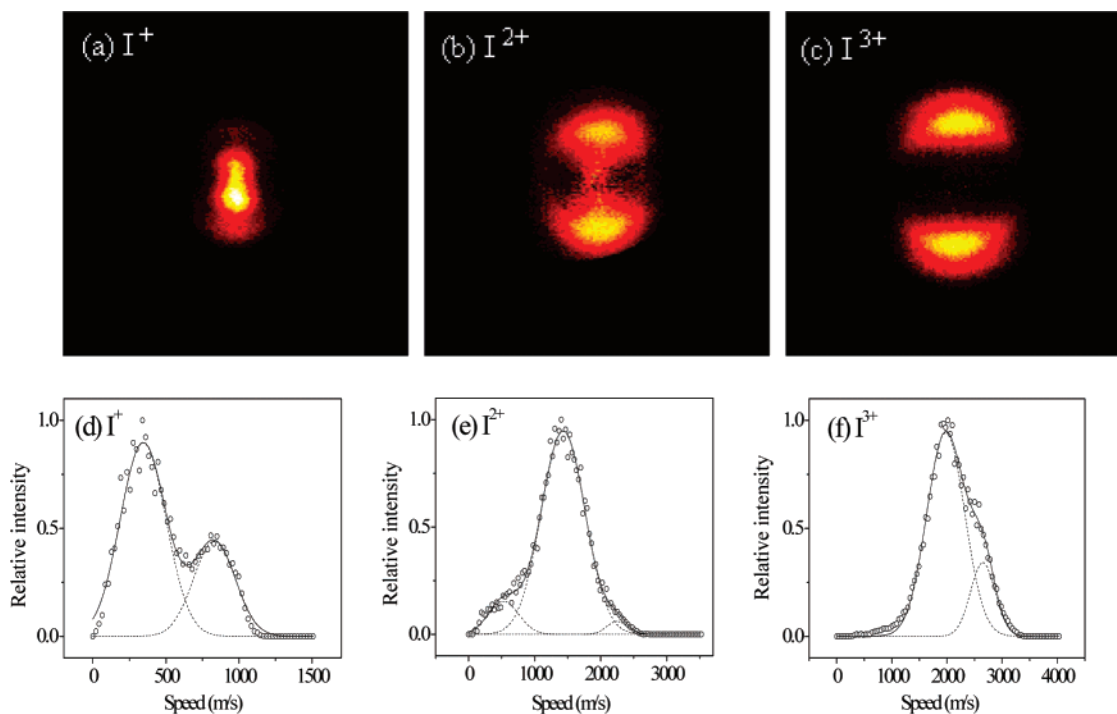


Figure 3. Images and speed distributions of I^+ , I^{2+} , and I^{3+} at a laser intensity of $6 \times 10^{14} \text{ W/cm}^2$.

using three Gaussian functions as shown in Figure 2. This indicates that multiple product channels are involved both for these two fragments. For CH_3^+ , three speed components were centered at 1409, 2865, and 3532 m/s, respectively. The corresponding CH_3^+ fragment translational energies were 0.15, 0.64, and 0.97 eV. For I^+ , three speed components centered at 208, 364, and 486 m/s were used for fitting. The corresponding fragment translational energies were 0.03, 0.09, and 0.16 eV. The speed distributions of the three iodine ions produced in

the Coulomb explosion also cannot be described by only one Gaussian function, indicating multichannel processes for these products. The $P(v)$ distribution of I^+ can be fitted with two Gaussian curves, which are centered at 344 and 832 m/s, while three Gaussian functions centered at 529, 1431, and 2246 m/s were used for I^{2+} . Two Gaussian fits centered at 1978 and 2651 m/s were used for I^{3+} . The fitting errors were smaller than 2.5%.

Expanding the angular distributions at the peak energies in a Legendre series

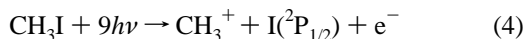
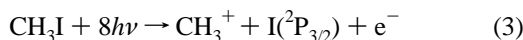
$$I(\theta) = \sum_s \beta_{2s} P_{2s}(\cos \theta) \quad (2)$$

we obtained $\beta_2 \geq 2$ for all the energy rings of the CH₃⁺ and I⁺ products of the dissociative ionization process. In addition, we obtained nonzero values of β_4 for almost all the rings. These anisotropy parameters are clear evidence of multiphoton absorption,²¹ which are coincident with previous analyses of the MPI mechanism. For the Coulomb explosion cases, the angular distributions of the iodine fragments are shown in Figure 4. The I^{q+} ion ($q = 1, 2,$ and 3) angular distributions are all of similar widths, which would imply a geometric, as opposed to dynamic, alignment. The angular distributions of the low-energy channel and the middle one for I²⁺ ions are so close that they have overlapped with each other.

4. Discussion

4.1. Dissociative Ionization of CH₃I. In our experiments, we used only one laser of 35 fs to excite the molecules. Considering the ionization process of polyatomic molecules⁵ is much faster than dissociation⁹ in a strong laser field, the neutral molecule CH₃I does not have enough time to be dissociated into neutral fragments. According to eq 1, the laser intensity of 8×10^{13} W/cm² is the turning point of the transition between MPI and FI mechanisms for CH₃I molecules in the case of 800 nm irradiation. What we have observed is a MPI dissociative ionization process at a laser intensity of 5×10^{13} W/cm². In the mass spectrum, the parent ion CH₃I⁺ was observed to be much stronger than the fragment ions CH₃⁺ and I⁺. From the energetic scheme of CH₃I, which is shown in Figure 5, the molecules in the ground state need to absorb seven photons to produce parent ions in two spin-orbit states of ²E_{3/2} and ²E_{1/2}. However, eight or nine photons need to be absorbed to enable dissociation to CH₃⁺ + I + e⁻ or CH₃ + I⁺ + e⁻ fragment channels. This is an explanation as to why the signal of CH₃I⁺ is much stronger than the fragments.

For the CH₃⁺ + I + e⁻ channel, the iodine fragment could be in the ground I(²P_{3/2}) or excited I*(²P_{1/2}) states. The \tilde{A} state, which corresponds to the CH₃ + I⁺ + e⁻ product channel, also could be led to the CH₃⁺ + I(²P_{3/2}) + e⁻ channel via internal conversion (I.C.). As such, the CH₃⁺ product could be from the possible channels as described as



The total energy, E_{avl} , available to the recoiling nuclei may be calculated from the appearance potential of the overall process. The appearance potential of channel 3 is 12.18 eV.²⁴ For channel 4, it is 13.12 eV. Considering the bandwidth of our laser pulse, the corresponding available energies of these two channels should be 0–0.54 and 0.49–1.19 eV, respectively. Comparing with our experimental values of 0.15, 0.64, and 0.97 eV, we can conclude that the low-speed component in Figure 2c is from channel 3. The molecules in the ground state absorb eight photons to reach the \tilde{A} excited state of parent ions and are converted via I.C. to the ground state of the ion and converge to the CH₃⁺ + I + e⁻ channel. The middle- and high-speed components are from channel 4. The molecules in the ground state absorb nine photons to reach the \tilde{B} excited state of the parent ions and converge to the CH₃⁺ + I* + e⁻ channel. Thus, the high-energy release channel centered at 0.97 eV observed for CH₃⁺ may originate from the photon absorption of the blue

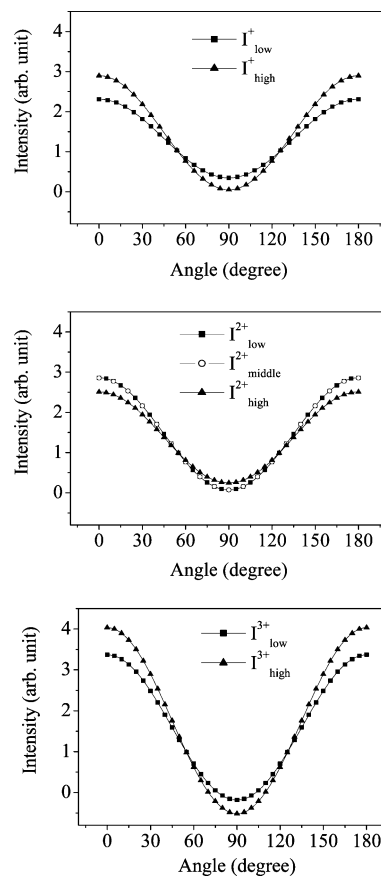


Figure 4. Angular distributions of I⁺, I²⁺, and I³⁺ at a laser intensity of 6×10^{14} W/cm².

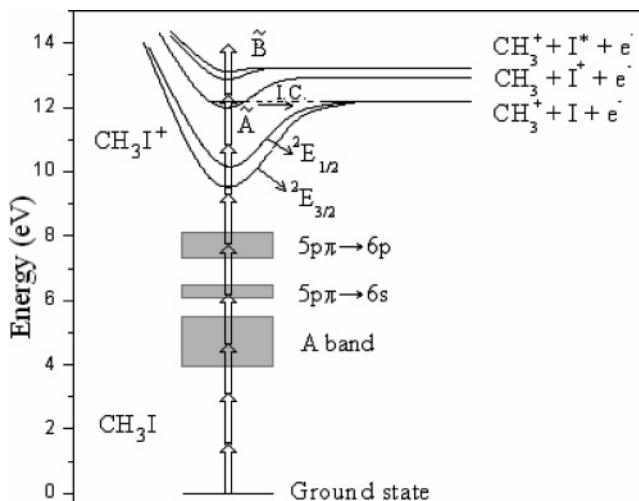
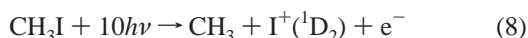
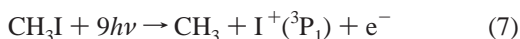
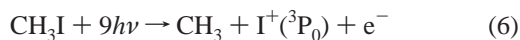
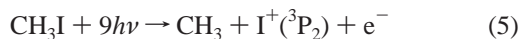


Figure 5. Energetic diagram of CH₃I, CH₃I⁺, and various dissociation channels. The energies of the states are taken from refs 22–25.

side of the excitation laser since our laser covers more than 40 nm width. If nine photons of 780 nm are absorbed in channel 4, the released kinetic energy of the dissociation should be ~ 1.19 eV, which is very similar to what we observed for the high-speed component in Figure 2c. We studied the mass spectra of the fragment ions recorded by a series of laser intensities attenuated successively at $\sim 10\%$, and we found that the KERs of the fragment ions were independent of the laser intensity. But, the relative intensity of different rings was changed. For example, the lowest speed channel became relatively stronger if we decreased the laser intensity to 4×10^{13} W/cm². This is

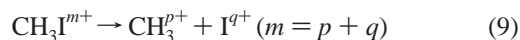
in agreement with the fact that the lowest channel coming from channel 3 needs to absorb one less photon than channel 4.

The I^+ ion coming from the $CH_3 + I^+ + e^-$ dissociation channel may be produced to different ionic states of 3P_2 , 3P_0 , 3P_1 , and 1D_2 .²⁶ The threshold energy for the production of the lowest $CH_3 + I^+(^3P_2) + e^-$ channel is 12.90 eV²⁴ as shown in Figure 5. For the higher channels in the production of $I^+(^3P_0)$, $I^+(^3P_1)$, and $I^+(^1D_2)$, the threshold energies were 13.70, 13.78, and 14.60 eV, respectively. The possible I^+ channels are listed as



Considering the bandwidth of the laser pulse, the available energies can be calculated to be 0.71–1.41, 0–0.61, 0–0.53, and 0.52–1.29 eV, respectively. The three translational energy components of I^+ are centered at 0.03, 0.09, and 0.16 eV, respectively. If we do not consider the recoil of the electron, that is, only two fragments are involved, then the released total translational energies calculated from the three speed components of I^+ should be 0.22, 0.68, and 1.21 eV in this limit condition. Then, the low-speed component of I^+ is possibly from channel 6 and 7. Since the available energies of these two channels are very close to each other, they cannot be distinguished further. The middle-speed component may come from channel 8. The high-speed component may come from nine photon absorption of the blue side of the excitation laser as channel 5 has described.

4.2. Coulomb Explosion of CH_3I . In the TOF mass spectra, multiply charged iodine ions I^{2+} and I^{3+} were observed except for singly charged CH_3I^+ , I^+ , CH_3^+ , and H^+ . These doubly and triply charged iodine ions were speculated as originating from the Coulomb explosion. Since the pulse duration is only 35 fs, it is unlikely that significant post-dissociation ionization occurs. Hence, the parent molecule is highly ionized, and then Coulomb explosion occurs to produce these multiply charged fragment ions. Although multiply charged parent ions were not observed directly, their role in the production of I^{q+} ($q \leq 3$) is inferred. The signal intensity of the iodine ion becomes weaker in turn with the charge increasing. From the fragments that we observed in the TOF-MS, the nonsequential multiple fragmentation channels are predicted as stated previously^{16,17}



The observed CH_3^+ ions can be produced from this two-body channel.

The KERs of the fragment ions produced by the Coulomb explosion are much larger than those in the case of dissociative ionization. The KERs of the fragments in a Coulomb explosion are from the repulsive Coulomb force, which depends on the charge of the fragments and the internuclear distance at which the fragments reach their final ionization state.

Experimentally, we obtained the kinetic energy of the fragments from the speed distributions following inversion of the measured images. For I^+ , the two speed components correspond to fragment kinetic energies of 0.08 and 0.46 eV, while for I^{2+} , the three kinetic energy components are 0.18,

1.35, and 3.32 eV. For I^{3+} , two components of 2.58 and 4.63 eV were obtained.

The KERs of the two fragments CH_3^{p+} and I^{q+} produced by the two-body dissociation channels have a relationship from the momentum conservation as follows:

$$KER(I^{q+})/KER(CH_3^{p+}) = M(CH_3^{p+})/M(I^{q+}) \quad (10)$$

where M is the mass of the fragment ions. Since the observed CH_3^+ ions can be from different precursors $CH_3^+I^{q+}$ ($q = 1, 2$, and 3) by the two-body dissociation channels, the CH_3^+ ions can be calculated to be 0.68 and 3.88 eV corresponding to the two speed components of its partner I^+ . The CH_3^+ ions with KERs of 1.52, 11.40, and 28.03 eV could be produced corresponding to I^{2+} . CH_3^+ ions with KERs of 21.78 and 39.09 eV may be produced simultaneously with I^{3+} . Obviously, most of the released kinetic energy in the explosion is carried away by the light part of CH_3^+ . The recoil speeds of CH_3^+ ions are very high. We tried to obtain the image of CH_3^+ ions, but they cannot be imaged fully in our detector. The very high translational energy releases do support our speculation of Coulomb explosion. The velocities of I^+ , I^{2+} , and I^{3+} increase in turn. This is because the production of iodine ions with more charges needs the parent molecule to be more highly ionized. The Coulomb repulsion force is thus much stronger for more multiply charged parent ions, and the higher charged fragments will obtain much more kinetic energy.

We can see that the images of three kinds of iodine ions have shown a very strong anisotropy along the laser polarization. This character has been commonplace in the Coulomb explosion process. The angular distributions of the three iodine fragments are similar in appearance, with comparable widths. The FWHM values of angular distributions of the I^+ , I^{2+} , and I^{3+} fragments are 90, 88, and 90°, respectively. The minimum intensity occurs at the 90° direction, and a maximum is shown in the laser polarization direction (0 and 180°). Because of its large moment of inertia and long rotational period (~1 ps), the CH_3I molecule is not expected to rotate significantly during the 35 fs pulse. Thus, the similar widths of about 90° of the angular distributions support that the observed anisotropy of the iodine ions results solely from the enhancement of the ionization and dissociation of these molecules, which are initially oriented along the laser polarization vector. This observation is similar to that described for the CS_2 molecule.²⁷ When the H_3-C-I bonds were orientated along the TOF axis, the I ions resulting from Coulomb explosion were detected efficiently, resulting in a maximum in the distribution.

5. Conclusion

The mass spectra, speed, and angular distributions of fragment ions from dissociative ionization and Coulomb explosion of the CH_3I molecule were studied at laser intensities of about 10^{13} and 10^{14} W/cm² with 35 fs laser pulses. Mass spectra of CH_3I at lower laser intensities of about 10^{13} W/cm² consisted of only three main mass peaks of CH_3I^+ , CH_3^+ , and I^+ . The speed distributions of CH_3^+ and I^+ were obtained using a velocity map imaging method. All speed distributions of these two fragments consisted of three components. The possible production channels were discussed. The fragment angular distributions showed a strong anisotropy along the laser polarization vector. The anisotropy parameters of the fragments support the MPI mechanism of the dissociative ionization process.

At higher laser intensities of about 6×10^{14} W/cm², multiply charged iodine ions were observed in the mass spectra. The

Coulomb explosion took place in the tunneling regime. The speed distributions of I^{q+} ($q \leq 3$) were obtained. All of them cannot be described by a single function resulting from the wave packet being projected onto different repulsive potentials. From the images of I⁺, I²⁺, and I³⁺, an obvious similar anisotropic character along the laser polarization was observed. The I^{q+} angular distributions were similar in appearance, with comparable FWHM values of about 90°. The maximum intensity occurred at 0 and 180°, which is parallel to laser polarization, and the minimum was at 90°. All of these phenomena indicate that geometric alignment dominated in these fragment-producing processes.

Acknowledgment. Support from the National Natural Science Foundation of China under Grants 10534010 and 20673140 is gratefully acknowledged.

References and Notes

- (1) Sharma, P.; Vasta, R. K.; Maity, D. K.; Kulshreshtha, S. K. *Chem. Phys. Lett.* **2003**, *382*, 637.
- (2) Vijayalakshmi, K.; Safvan, C. P.; Ravindra, K. G.; Mathur, D. *Chem. Phys. Lett.* **1997**, *270*, 37.
- (3) Wu, C.-Y.; Xiong, Y.-J.; Ji, N.; He, Y.; Gao, Z.; Kong, F. *J. Phys. Chem. A* **2001**, *105*, 374.
- (4) Unny, S.; Du, Y.; Zhu, L.; Gordon, R. J. *Phys. Rev. Lett.* **2001**, *86*, 2245.
- (5) Tzallas, P.; Kosmidis, C.; Philis, J. G.; Ledingham, K. W. D.; McCanny, T.; Singhal, R. P.; Hankin, S. M.; Taday, P. F.; Langley, A. J. *Chem. Phys. Lett.* **2001**, *343*, 91.
- (6) Siozos, P.; Kaziannis, S.; Kosmidis, C. *Int. J. Mass Spectrosc.* **2003**, *225*, 249.
- (7) Berry, R. S.; Leach, S. *Adv. Electron. Electron. Phys.* **1980**, *57*, 119.
- (8) Seideman, T.; Ivanov, M. Y.; Corkum, P. B. *Phys. Rev. Lett.* **1995**, *75*, 2819.
- (9) Castillejo, M.; Martin, M.; De Nalda, R.; Couris, S.; Koudoumas, E. *Chem. Phys. Lett.* **2002**, *353*, 295.
- (10) Eppink, A. T. J. B.; Parker, D. H. *J. Chem. Phys.* **1998**, *109*, 4758.
- (11) Jung, Y.-J.; Kim, Y. S.; Kang, W. K.; Jung, K.-H. *J. Chem. Phys.* **1997**, *107*, 7187.
- (12) Van den Brom, A. J.; Lipciuc, M. L.; Janssen, M. H. M. *Chem. Phys. Lett.* **2003**, *368*, 324.
- (13) Samartzis, P. C.; Bakker, B. L. G.; Parker, D. H.; Kitsopoulos, T. N. *J. Phys. Chem. A* **1999**, *103*, 6106.
- (14) Graham, P.; Ledingham, K. W. D.; Singhal, R. P.; Hankin, S. M.; McCanny, T.; Fang, X.; Kosmidis, C.; Tzallas, P.; Taday, P. F.; Langley, A. J. *J. Phys. B: At., Mol. Opt. Phys.* **2001**, *34*, 4015.
- (15) Ma, R.; Wu, C.; Xu, N.; Huang, J.; Yang, H.; Gong, Q. *Chem. Phys. Lett.* **2005**, *415*, 58.
- (16) Kaziannis, S.; Siozos, P.; Kosmidis, C. *Chem. Phys. Lett.* **2005**, *401*, 115.
- (17) Liu, H.; Zheng, Y.; Gao, Z.; Tang, Z. *J. Chem. Phys.* **2007**, *126*, 44316.
- (18) Eppink, A. T. J. B.; Parker, D. H. *Rev. Sci. Instrum.* **1997**, *68*, 3477.
- (19) Parker, D. H.; Eppink, A. T. J. B. *J. Chem. Phys.* **1997**, *107*, 2357.
- (20) Zhang, S.; Wang, Y.; Tang, B.; Zheng, Q.; Zhang, B. *Chem. Phys. Lett.* **2005**, *413*, 129.
- (21) Gordon, R. G.; Hall, G. E. *Adv. Chem. Phys.* **1996**, *96*, 1.
- (22) Gedanken, A.; Robin, M. B.; Yafet, Y. *J. Chem. Phys.* **1982**, *76*, 4798.
- (23) Strobel, A.; Fischer, I.; Lochschmidt, A.; Müller-Dethlefs, K.; Bondybey, V. E. *J. Phys. Chem.* **1994**, *98*, 2024.
- (24) NIST Chemistry Webbook, <http://webbook.nist.gov/chemistry>.
- (25) Walter, K.; Weinkauff, R.; Boesl, U.; Schlag, E. W. *J. Chem. Phys.* **1988**, *89*, 1914.
- (26) Pratt, S. T. *Phys. Rev. A: At., Mol., Opt. Phys.* **1986**, *33*, 1718.
- (27) Graham, P.; Ledingham, K. W. D.; Singhal, R. P.; McCanny, T.; Hankin, S. M.; Fang, X.; Smith, D. J.; Kosmidis, C.; Tzallas, P.; Langley, A. J.; Taday, P. F. *J. Phys. B: At., Mol. Opt. Phys.* **1999**, *32*, 5557.